Earth Planet. Sci. Lett. 648 (2024) 119111

Contents lists available at ScienceDirect

Earth and Planetary Science Letters

journal homepage: www.elsevier.com/locate/epsl

Unsteady slip pulses under spatially-varying prestress

Anna Pomyalov, Eran Bouchbinder *

Chemical and Biological Physics Department, Weizmann Institute of Science, Rehovot 7610001, Israel

ARTICLE INFO

Editor: C. Lithgow-Bertelloni

Keywords:
Slip pulses
Nonuniform prestress
Reduced-dimensionality descriptions
Back-propagating rupture
Pulse-to-crack transition

ABSTRACT

It has been recently established that self-healing slip pulses under uniform background/ambient stress (prestress) τ_b are intrinsically unstable frictional rupture modes, i.e., they either slowly expand or decay with time t. Furthermore, their spatiotemporal dynamics have been shown to follow a reduced-dimensionality description corresponding to a special one-dimensional curve $L(c)$, parameterized by τ_b, in a plane defined by the pulse propagation velocity $c(t)$ and size $L(t)$. Yet, uniform prestress is rather the exception than the rule in natural faults. Here, we study the effects of a spatially-varying prestress $\tau_b(x)$ (in the fault direction x) on 2D slip pulses, initially generated under a uniform τ_b along a rate-and-state friction fault. We consider both periodic and constant-gradient prestress distributions $\tau_b(x)$ around the reference uniform τ_b. For a periodic $\tau_b(x)$, pulses either sustain and form quasi-limit cycles in the $L-c$ plane or decay predominantly monotonically along the $L(c)$ curve depending on the instability index of the initial pulse and the properties of the periodic $\tau_b(x)$. For a constant-gradient $\tau_b(x)$, expanding and decaying pulses closely follow the $L(c)$ curve, with small systematic shifts determined by the sign and magnitude of the gradient. We also find that a spatially-varying $\tau_b(x)$ can revert the expanding/decaying nature of the initial reference pulse. Finally, we show that a constant-gradient $\tau_b(x)$, of sufficient magnitude and specific sign, can lead to the nucleation of a back-propagating rupture at the healing tail of the initial pulse, generating a bilateral crack-like rupture. This pulse-to-crack transition, along with the above-described effects, demonstrates that rather rich rupture dynamics can emerge from a simple, spatially-varying prestress. Furthermore, our results show that as long as pulses exist, their spatiotemporal dynamics are related to the special $L(c)$ curve, providing an effective, reduced-dimensionality description of unsteady slip pulses under spatially-varying prestress.

1. Background and motivation

Classical models of earthquakes, which consider a single frictional rupture that propagates along a homogeneous and planar fault separating unbounded linear elastic blocks in the presence of a uniform background/ambient stress (prestress) τ_b, offer insight into the physics and mechanics of faulting (Freund, 1998; Rice, 1980; Scholz, 2002). Single frictional rupture is classified into crack-like modes and self-healing slip pulses (Brener et al., 2018; Gabriel et al., 2012; Heaton, 1990; Lu et al., 2007; Perrin et al., 1995), where the latter feature a characteristic size L that implies a finite slip duration at points along the fault. Yet, our understanding of even these relatively simple models is incomplete.

Major recent progress has been made in understanding the spatiotemporal dynamics of self-healing slip pulses propagating along rate-and-state friction faults under a uniform prestress τ_b (Pomyalov et al., 2023a). It has been shown that slip pulses are intrinsically unstable objects that cannot propagate steadily, i.e., they either expand ($\dot{L}(t) > 0$) or decay ($\dot{L}(t) < 0$) with increasing time t. Yet, it has been shown that the unsteady pulses dynamics are slow and follow a special one-dimensional curve $L(c)$ in a plane defined by the pulse propagation velocity $c(t)$ and size $L(t)$. The special $L(c)$ curve corresponds to steady pulse solutions parameterized by τ_b, which is composed of unstable points that nevertheless form a dynamic attractor at a given τ_b. As such, the special $L(c)$ curve should be regarded as an equation of motion for unsteady pulses under uniform prestress. This reduced-dimensionality description remains valid for other pairs of pulse quantities, e.g., the peak slip velocity $v_p(t)$ and $L(t)$ (Pomyalov et al., 2023a).

Real faults in the earth crust generally feature spatially-varying prestress (Aki, 1979; Bache et al., 1980; Beroza and Mikumo, 1996; Hanks, 1974; Hartzell and Brune, 1979; Kanamori and Stewart, 1978; Matsumoto et al., 2018; Mildon et al., 2019). Such nonuniform prestress distributions may emerge from previous inhomogeneous slip histories, or to effectively mimic either spatial variations in the frictional strength or geometrical fault irregularities. The latter include barri-

* Corresponding author.
E-mail address: eran.bouchbinder@weizmann.ac.il (E. Bouchbinder).

https://doi.org/10.1016/j.epsl.2024.119111
Received 31 July 2024; Received in revised form 30 October 2024; Accepted 1 November 2024
Available online 6 November 2024

ers (Aki, 1979), bends (Mildon et al., 2019), double fault bends (Lozos et al., 2011), branched fault systems (Duan and Oglesby, 2007) and fault surface roughness (Fang and Dunham, 2013; Heimisson, 2020). Consequently, it has been recognized quite a long time ago that earthquake models should be extended to include spatially-varying prestress distributions (Aki, 1979; Day, 1982). It is particularly interesting to understand whether and to what extent a nonuniform prestress may contribute to the emergence of slip complexity, including phenomena such as non-self-healing slip pulses (Beroza and Mikumo, 1996), rupture arrest, back-propagating rupture (Ding et al., 2024; Idini and Ampuero, 2020) and pulse-to-crack transitions (Brantut et al., 2019; Brener et al., 2018; Gabriel et al., 2012; Heimisson, 2020; Lu et al., 2007; Perrin et al., 1995).

Indeed, some works have studied the effects of nonuniform prestress on frictional rupture dynamics in various spatial dimensionalities, including in three dimensions (3D) (Day, 1982), in two dimensions (2D) (Elbanna, 2011; Johnson, 1990) and in one dimensional (1D) space (Barras et al., 2023), to list a few among others. The PhD thesis of Elbanna (2011) (see chapter 5 therein) focused on 2D pulse propagation in nonuniform prestress fields, arguing that the interaction of pulses with inhomogeneous prestress distributions is of particular interest as the finite size of pulses implies larger sensitivity to prestress spatial variations compared to crack-like rupture, which may tend to smooth out their effect.

Our goal in this paper is to study 2D unsteady pulse dynamics under spatially-varying prestress distributions $\tau_b(x)$ of two classes, both varying slowly compared to the pulse's size. One is a periodic prestress and the other is a constant-gradient prestress. We will employ the above-mentioned reduced-dimensionality description of unsteady slip pulses, originally developed under uniform prestress (Pomyalov et al., 2023a), to quantify pulse dynamics under nonuniform $\tau_b(x)$ and to test the degree by which this theoretical framework extends to a broader class of problems. Our analysis also employs well-defined initial pulse states, corresponding to controllably perturbed steady-state pulse solutions.

2. Problem setup: initial pulses and the spatially-varying prestress $\tau_b(x)$

We consider slip dynamics along a rate-and-state friction fault separating two infinite linear elastic blocks under anti-plane shear. The displacement field is $u_z(x,y,t)$, where $y=0$ defines the fault and z is perpendicular to the xy plane. The frictional strength $\tau(v,\phi)$ is a functional of the slip velocity field $v(x,t) \equiv 2\partial_t u_z(x, y=0^+, t)$ and of the state field $\phi(x,t)$. The latter follows the "aging law" $\partial_t \phi(x,t) = 1 - v(x,t)\,\phi(x,t)/D$, where D is a characteristic slip displacement (Baumberger and Caroli, 2006; Dieterich, 1979; Marone, 1998; Nakatani, 2001; Ruina, 1983). $\tau(v,\phi)$, whose explicit expression is given in the Supplementary Material (SM, see Eq. (S1) therein), features an N shape under steady-state sliding (for which $\phi = D/v$), with a transition from rate-weakening to rate-strengthening friction occurring at a local minimum $(v_{\min}, \tau_{\min})$ of the steady-state friction strength (see SM).

Spatiotemporal slip dynamics for $t > 0$ are described by the boundary integral equation (Das, 1980)

$$\tau[v(x,t), \phi(x,t)] = \tau_b(x) - \frac{\mu}{2c_s} v(x,t) + s(x,t)\ , \tag{1}$$

balancing the frictional strength on the left-hand-side with the interfacial shear stress on the right-hand-side. The latter features three contributions; the first is the spatially-varying prestress $\tau_b(x)$, the second is the so-called radiation-damping term (where μ is the shear modulus and c_s is the shear wave-speed) and the third, $s(x,t)$, is a spatiotemporal convolutional integral that accounts for the long-range interaction of different parts of the fault, mediated by bulk elastodynamic deformation. Equation (1), along with the ϕ evolution equation, is solved in the spectral domain (Breitenfeld and Geubelle, 1998) using the open-source library *cRacklet* (Roch et al., 2022) in a periodic domain of size W, i.e., $x \in [-\frac{1}{2}W, \frac{1}{2}W]$ with periodic boundary conditions (see SM). The problem formulation is completed once the initial conditions and $\tau_b(x)$ are specified.

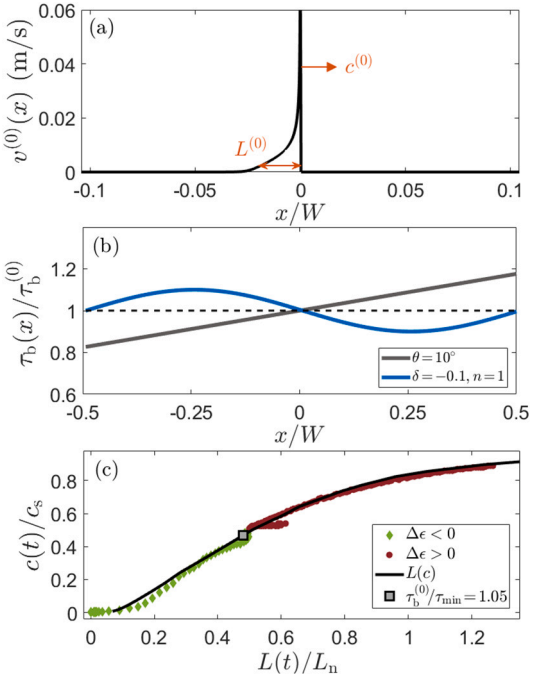

Fig. 1. (a) The slip velocity field $v^{(0)}(x)$ of a steady-state slip pulse characterized by size $L^{(0)}$ (marked) and propagation velocity $c^{(0)}$ (from left to right, marked). $x = 0$ corresponds to the location of the peak slip velocity v_p (not marked). (b) Examples of members of the two nonuniform prestress $\tau_b(x)$ classes discussed in the text (see legend for the parameters). Note that while $x = 0$ here is aligned with $x = 0$ of panel (a), there is an order of magnitude difference in the x axis range of the two panels. (c) Unsteady slip pulse dynamics under uniform prestress $\tau_b^{(0)}/\tau_{\min} = 1.05$, presented in the $L-c$ plane (L_n is a normalization length, see SM). The special curve $L(c)$ is marked by the solid line (Pomyalov et al., 2023a). The steady-state pulse corresponding to $\tau_b^{(0)}/\tau_{\min} = 1.05$, marked by the square, is initially perturbed with $\Delta\epsilon > 0$ (brown circles) or with $\Delta\epsilon < 0$ (green diamonds), and their subsequent evolution ($t > 0$) is plotted in the $L-c$ plane. As extensively discussed in Pomyalov et al. (2023a), unsteady pulse dynamics closely follow the steady-state $L(c)$, whether the pulse expands ($\Delta\epsilon > 0$) or decays ($\Delta\epsilon < 0$).

In setting up the initial conditions, our goal is to employ well-defined and controlled states that will allow us to address our main question regarding the interaction of slip pulses with nonuniform prestress distributions. Consequently, we are not interested in spontaneous frictional rupture nucleation under nonuniform prestress, but rather in generating propagating self-healing slip pulses with known properties. To this end, we invoke the steady-state pulse solutions of Pomyalov et al. (2023b), obtained under a uniform prestress, to be denoted as $\tau_b^{(0)}$. Each such solution is characterized by time-independent slip velocity $v^{(0)}(x)$ and state $\phi^{(0)}(x)$ fields, which propagate steadily at a velocity $c^{(0)}$ and feature a characteristic size $L^{(0)}$, see Fig. 1a.

Such solutions were shown to correspond to "saddle configurations" separating expanding from decaying pulses. This implies that small positive perturbations of the steady-state pulse, which we quantify through an instability index $\Delta\epsilon > 0$ (for a formal definition see SM), lead to a growing pulse, while small negative perturbations of the steady-state pulse with $\Delta\epsilon < 0$, lead to a decaying pulse, where $|\Delta\epsilon|$ determines the initial rate of instability. As such, $\Delta\epsilon$ quantifies the degree and nature/sign of the unsteadiness of the initial slip pulses under uniform prestress. Consequently, it allows us to disentangle the dynamical effects of the intrinsic unsteady nature of slip pulses from those of a spatially-varying prestress, as is further discussed and demonstrated below.

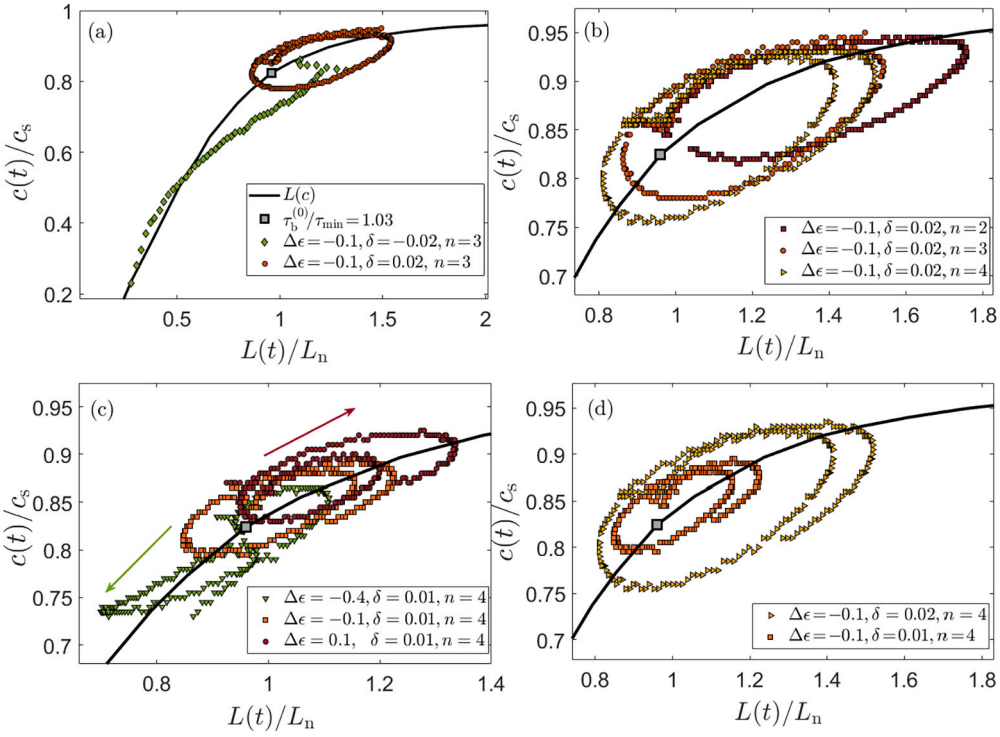

Fig. 2. Unsteady pulse dynamics under periodic prestress $\tau_b(x)$ of Eq. (2), with fault average $\langle\tau_b(x)\rangle_x/\tau_{min}=1.03$. In all panels, the square represents the $\tau_b^{(0)}/\tau_{min}=1.03$ steady-state pulse and the black line represents the special $L(c)$ curve in the $L-c$ plane. (a) Pulse dynamics for $\Delta\epsilon=-0.1$ and $n=3$, with $\delta=0.02$ (orange circles) and $\delta=-0.02$ (green diamonds). See legend and text for discussion. (b) Pulse dynamics for $\Delta\epsilon=-0.1$ and $\delta=0.02$, with different prestress wavelengths $\lambda=W/n$ (varied through n). See legend and text for discussion. (c) Pulse dynamics for $\delta=0.01$ and $n=4$, with different initial instability indices $\Delta\epsilon$ (see legend). The green and brown arrows indicate the overall direction of the pulse trajectory in the $L-c$ plane. See text for discussion. (d) Pulse dynamics for $\Delta\epsilon=-0.1$ and $n=4$, with different positive amplitudes $\delta>0$ (see legend and text for discussion).

Yet another major advantage of using controllably perturbed steady-state pulses, obtained under uniform prestress $\tau_b^{(0)}$, as initial conditions for Eq. (1), is that they set a dynamical reference for the analysis under spatially-varying prestress $\tau_b(x)$ to follow. Specifically, as already stated, it has been recently demonstrated that the unsteady pulse motion under uniform prestress $\tau_b^{(0)}$, e.g., as quantified by the time evolution of $L(t)$ and $c(t)$, closely follows the special $L(c)$ curve in the $L-c$ plane, whether the pulse grows/expands ($\dot{L}(t)>0$ for $\Delta\epsilon>0$) or decays ($\dot{L}(t)<0$ for $\Delta\epsilon<0$), see Fig. 1c. The special $L(c)$ curve, which corresponds to steady-state pulse solutions parameterized by $\tau_b^{(0)}$ (Pomyalov et al., 2023b), has been shown to be a dynamic attractor (also for pulses nucleated away from it) and hence to provide a reduced-dimensionality description of unsteady slip pulses under uniform prestress (Pomyalov et al., 2023a). The degree by which this reduced-dimensionality description extends to unsteady pulse dynamics under spatially-varying prestress is a central question addressed in this work.

To complete the problem formulation, we need to specify the spatially-varying prestress distributions $\tau_b(x)$ in Eq. (1). A first class of prestress distributions corresponds to a periodic (sinusoidal) variation of the form

$$\tau_b(x)=\tau_b^{(0)}\left[1+\delta\sin(2\pi n x/W)\right]\ . \tag{2}$$

Here, the prestress distribution is characterized by two parameters: a dimensionless amplitude δ and a wavelength $\lambda=W/n$ determined by n (expressed in terms of the domain size W). A second class of prestress distributions corresponds to a constant spatial gradient $d\tau_b(x)/dx$ that is characterized by a tilt angle θ according to

$$\tau_b(x)=\tau_b^{(0)}\left[1+2\tan(\theta)\,x/W\right]\ , \tag{3}$$

where $\theta>0$ corresponds to a counterclockwise tilt. Examples of members of the two $\tau_b(x)$ classes are shown in Fig. 1b.

The fault average, — i.e., the spatial average over the entire fault $-W/2\le x\le W/2$ — of both distributions in Eqs. (2)-(3) satisfies $\langle\tau_b(x)\rangle_x=\tau_b^{(0)}$, where the latter characterizes the uniform prestress for which the perturbed steady-state (serving as the $t=0$ initial condition) was obtained. This setup mimics physical situations in which an unsteady slip pulse obtained under a uniform prestress $\tau_b^{(0)}$ enters at $t=0^+$ a region of nonuniform prestress $\tau_b(x)$ (with a fault average that equals $\tau_b^{(0)}$), and its subsequent $t>0$ dynamics are tracked. Note also, as stated above, that we are interested in prestress distributions that vary rather slowly on the characteristic scale $L^{(0)}$ (the size of the initial slip pulse). In the other limit, where the characteristic spatial scale of variation of $\tau_b(x)$ is smaller than $L^{(0)}$, we expect the pulse to smooth out the spatial variability of the prestress (see Sect. S-3B in the SM).

3. Pulse dynamics under periodic prestress

We first consider the periodic prestress distributions in Eq. (2). We set $\langle\tau_b(x)\rangle_x/\tau_{min}=1.03$ and study pulse dynamics in a system with $W=480$ m, for various $\Delta\epsilon$, δ and n. In Fig. 2a, we present the pulse dynamics in the $L-c$ plane for $\Delta\epsilon=-0.1$, i.e., a pulse that decays under a uniform prestress. For $\delta=0.02$ and $n=3$, it is observed that the pulse sustains, instead of decaying, and forms a limit cycle in the $L-c$ plane (orange circles). The limit cycle, which is a manifestation of the periodic prestress, corresponds to a pulse whose $L(t)$ and $c(t)$ vary nearly periodically as it propagates (see Fig. S4 in the SM). It remains close to the special $L(c)$ curve (solid black line) and encircles the corresponding uniform prestress fixed point (square). In this case, the periodic prestress transforms a decaying pulse (obtained under a uniform prestress corresponding to the fault average of the periodic one) into a long-lived, sustained pulse. Changing the overall sign of the periodic prestress (i.e., setting $\delta=-0.02$), leads to a decaying pulse, which closely follows the special $L(c)$ curve (green diamonds). These results indicate that the gra-

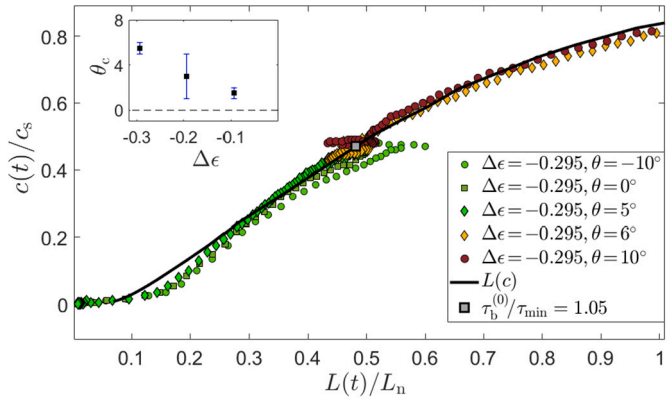

Fig. 3. Unsteady pulse dynamics under constant-gradient prestress $\tau_b(x)$ of Eq. (3), with fault average $\langle\tau_b(x)\rangle_x/\tau_{min}=1.05$. Results for $\Delta\epsilon=-0.295$ and various tilt angles in the range $-10°\le\theta\le 10°$ are presented, see legend and text for discussion. (inset) The threshold tilt angle $\theta_c>0$ (with error bars), required to induce a transition from decaying to growing/expanding pulses, as a function of $\Delta\epsilon<0$. The space-time manifestation of the transition is shown in Fig. S6 in the SM.

dient of $\tau_b(x)$ near $x=0$, in particular its sign, plays an important role in determining the fate of the pulse (i.e., whether it decays or sustains and follows a limit cycle in the L–c plane).

In Fig. 2b, we set $\Delta\epsilon=-0.1$ and $\delta=0.02$, and vary the wavelength of the periodic prestress (by setting $n=2,3,4$, see legend). It is observed that sustained pulses, forming quasi-limit cycles in the L–c plane close to the special $L(c)$ curve, emerge. The quasi-limit cycles are pushed to larger L and c values with increasing wavelength (decreasing n). We use the term "quasi-limit cycle" as in some cases the limit cycle is not exact and since we did not always follow the dynamics over very long times (and system sizes W), due to computational constraints; consequently, we cannot always determine whether the limit cycle is exact or approximate (e.g., drifts with increasing time, see Fig. S4 in the SM).

In Fig. 2c, we fix the periodic prestress parameters $\delta=0.01$ and $n=4$, and vary the instability index $\Delta\epsilon$ of the initial pulse. For $\Delta\epsilon=0.1$ (brown cycles), a quasi-limit cycle close to the special $L(c)$ curve emerges (the cycle in the L–c plane seems to be drifting upwards with time). Upon decreasing $\Delta\epsilon$, setting it to $\Delta\epsilon=-0.1$ (orange squares), a quasi-limit cycle also appears to emerge (recall that $\delta>0$). Upon further decreasing $\Delta\epsilon$, setting it to $\Delta\epsilon=-0.4$ (green triangles), the pulse initially attempts to form a limit cycle in the L–c plane, but appears to be drifting to smaller L and c values, and to decay. Finally, in Fig. 2d, we fix $\Delta\epsilon=-0.1$ and $n=4$, and vary the amplitude $\delta>0$ of the periodic prestress (see legend). It is observed that the emerging quasi-limit cycle broadens with increasing $\delta>0$. Overall, the results presented in Fig. 2 indicate that a periodic prestress distribution can reverse the fate of the original pulse (under uniform prestress), leading to either decaying pulses or to quasi-limit cycles in the L–c plane. In both cases, for the parameters considered, the unsteady pulse dynamics remain rather close to the special $L(c)$ curve, which corresponds to steady-state pulse solutions parameterized by a uniform prestress $\tau_b^{(0)}$ (Pomyalov et al., 2023a).

4. Pulse dynamics under constant-gradient prestress

We next consider the constant-gradient prestress distributions in Eq. (3). We set $\langle\tau_b(x)\rangle_x/\tau_{min}=1.05$ and study pulse dynamics in a system with $W=480$ m, for various instability indices $\Delta\epsilon$ and tilt angles θ. In Fig. 3, we present the pulse dynamics in the L–c plane for $\Delta\epsilon=-0.295$, i.e., a pulse that decays under a uniform prestress (corresponding to $\theta=0°$ in the figure, see green squares), and various values of θ. Upon imposing a negative prestress gradient, corresponding to $\theta=-10°$ (green circles), the pulse decays with a small down shift compared to the reference $\theta=0°$ results, yet it still follows rather closely the special $L(c)$ curve (solid black line). Upon imposing a positive prestress gradient of $\theta=5°$ (green diamonds), the pulse decays with a small up shift compared to the reference $\theta=0°$ results.

The dynamics qualitatively change upon setting $\theta=6°$ (yellow diamonds), where the pulse changes its character and becomes a growing/expanding pulse, which closely follows the special $L(c)$ curve. A similar growing/expanding pulse is observed for $\theta=10°$ (brown circles), featuring a small up shift compared to the $\theta=6°$ results. These results indicate that for a given instability index $\Delta\epsilon<0$, there exists a threshold tilt angle $\theta_c>0$ that can reverse the nature/fate of the pulse, from decaying to growing. For $\Delta\epsilon=-0.295$, θ_c is between 5° and 6°. In the inset of Fig. 3, we plot θ_c against $\Delta\epsilon<0$, demonstrating that there is an interplay between the instability index of the initial pulse and the threshold tilt angle $\theta_c>0$ needed to induce a transition from decaying to growing/expanding pulses. The space-time manifestation of the transition is shown in Fig. S6 in the SM.

Our analysis above focused on initial self-healing slip pulses that remain pulses under various spatially-varying prestress conditions. Yet, as noted in Sect. 1, earthquakes can take the form of either pulse-like or crack-like rupture, with significant implications for the duration of slip, earthquake energy budget, rupture scaling laws and seismic radiation. The dynamic selection of these rupture modes/styles and the spontaneous transition between them are important topics under active investigation, e.g., see Brantut et al. (2019); Brener et al. (2018); Gabriel et al. (2012); Heimisson (2020); Lu et al. (2007); Perrin et al. (1995). It is generally established (Brantut et al., 2019; Brener et al., 2018; Gabriel et al., 2012; Lu et al., 2007; Perrin et al., 1995) that crack-like rupture is more prevalent under larger average prestress levels. Consequently, it would be interesting to see whether for $\langle\tau_b(x)\rangle_x/\tau_{min}=1.05$ (a higher average prestress compared to the one considered in Sect. 3), a spatially-varying prestress distribution can spontaneously induce a pulse-to-crack rupture transition.

To address this question, we present in Fig. 4 (top row) a series of equal-time snapshots of $v(x,t)$ (Fig. 4a) and $\tau(x,t)$ (Fig. 4b) obtained for $\langle\tau_b(x)\rangle_x/\tau_{min}=1.05$ and $\Delta\epsilon=0.005$, under a constant-gradient prestress with $\theta=-9°$. It is observed that the nonuniform prestress transforms a growing pulse ($\Delta\epsilon>0$) into a decaying pulse, which propagates a certain distance from left to right (in the positive x direction), until it arrests/dies off. Note that pulse arrest leaves behind it a heterogeneous stress distribution (brightest, rightmost snapshot in panel (b)). Interestingly, it is observed that near the healing tail of the initial pulse, around $x/W\simeq -0.03$ (also marked by an arrow), there seems to be a spontaneous attempt to nucleate secondary rupture. The latter is evident in $\tau(x,t)$ (Fig. 4b), but requires a logarithmic scale to be discerned in $v(x,t)$, as done in the inset of Fig. 4a.

In Fig. 4 (bottom row), we present the spatiotemporal dynamics for a slightly stronger negative gradient, corresponding to $\theta=-10°$ (everything else being the same as in the top row). It is observed that this nonuniform prestress leads to a qualitative change in the dynamics. First, the attempted nucleation near the healing tail of the initial pulse, around $x/W\simeq -0.03$, becomes a successful nucleation event, giving rise to an asymmetric bilateral crack-like rupture. The rupture edge that propagates from right to left (in the negative x direction) corresponds to a back-propagating rupture. The rupture edge propagating in the forward (positive x) direction, catches up with the initial pulse that also propagates in the forward direction and merges with it. Second, upon merging of the two forward-propagating rupture fronts, a persistent asymmetric bilateral crack-like rupture emerges. Overall, it is observed that a spatially-varying prestress can induce a pulse-to-crack transition.

The crack-like nature of the two persistent, oppositely propagating rupture edges is evident in the inset of Fig. 4c (note the logarithmic y-axis), where a persistent finite slip velocity is left in the central part, while the two oppositely propagating rupture edges move further away. Similarly, the crack-like nature of the emerging rupture is also manifested in the residual stress observed in Fig. 4d. These results, which are presented again in a space-time plot in Fig. 5, demonstrate that

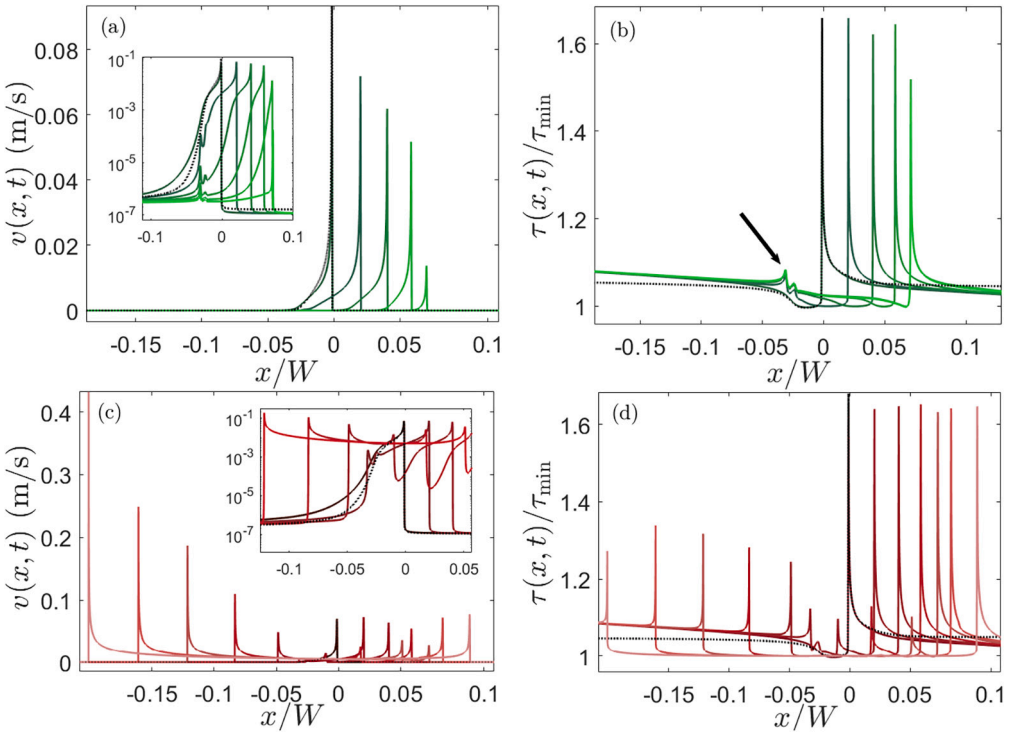

Fig. 4. A series of equal-time snapshots of the slip velocity field $v(x,t)$ (left column) and shear stress field $\tau(x,t)$ (right column), obtained for $\langle\tau_b(x)\rangle_x/\tau_{\min} = 1.05$ and an initial pulse with $\Delta\epsilon = 0.005$ (shown in a dotted black line in each panel), under a constant-gradient prestress with $\theta = -9°$ (top row) and $\theta = -10°$ (bottom row). Time evolves from darker to lighter colors, also revealing the direction of rupture propagation. The insets in panels (a) and (c) present a spatial zoom-in of the main panels, and employ a logarithmic y-axis for the slip velocity field $v(x,t)$. Note also that pulse arrest leaves behind it a heterogeneous stress distribution (brightest, rightmost snapshot in panel (b)). The presented results are extensively discussed in the text. See also Fig. 5, which presents the results of panel (c) in a space-time plot.

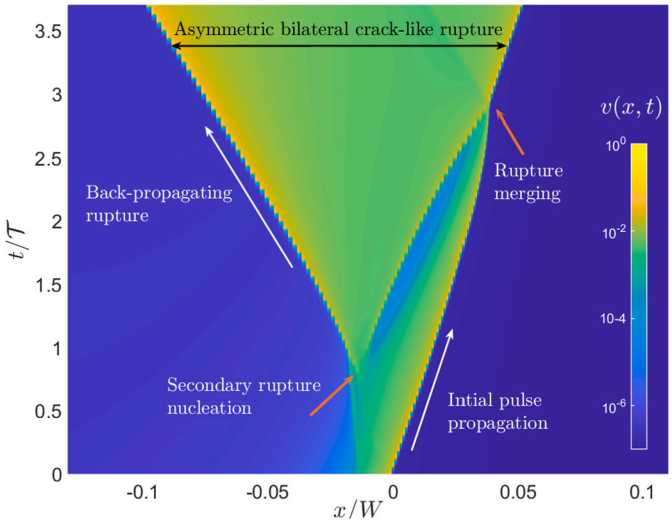

Fig. 5. Results of the same computation as in Fig. 4c-d, presented here in a space-time x–t plot. The slip velocity field $v(x,t)$ (in units of m/s, as in Fig. 4c) is plotted on a logarithmic scale, see color legend on the right. x is normalized by the fault size W and t by $\mathcal{T} \equiv L^{(0)}/c^{(0)}$. All dynamical events and various rupture propagation modes are marked, see text for additional discussion.

rich spatiotemporal rupture dynamics may emerge from rather simple spatially-varying prestress distributions, revealing phenomena such as back-propagating rupture and pulse-to-crack transitions, which are of interest in various geophysical contexts, e.g., in relation to earthquake source models and seismological inversion analyses (Ding et al., 2024; Idini and Ampuero, 2020). Finally, we note — as highlighted in Pomyalov et al. (2023a) — that once pulse-like rupture transforms into a crack-like rupture, the dynamics of latter can no longer be meaningfully represented in the L–c plane and an intrinsic relation to the special $L(c)$ curve — which is essentially an equation of motion for self-healing slip pulses under uniform prestress — does not exist anymore.

5. Summary and concluding remarks

In this paper, we studied the interaction of well-defined initial self-healing slip pulses with two classes of spatially-varying prestress distributions $\tau_b(x)$, one corresponding to a periodic variation and one to a constant gradient, see Eqs. (2)-(3). Our findings can be summarized along two major axes. The first concerns the richness (or to some extent the complexity) of rupture dynamics emerging from initial slip pulses interacting with a spatially-varying prestress (compared to their uniform prestress counterparts). The second concerns the theoretical description of unsteady slip pulse dynamics under spatially-varying prestress, particularly in relation to the recently established reduced-dimensionality description of pulse dynamics (Pomyalov et al., 2023a).

We have demonstrated that simple nonuniform prestress distributions can give rise to rather rich rupture dynamics. In particular, we showed that a nonuniform prestress can reverse the nature/fate of a slip pulse, from decaying/shrinking to growing/expanding and vice versa, for a fixed fault-averaged prestress, see Figs. 2-3. We also showed that pulses under periodic prestress can settle into propagating states in which their properties, e.g., pulse size $L(t)$, peak slip velocity $v_p(t)$ and propagation velocity $c(t)$, vary periodically or quasi-periodically as they propagate. Finally, we demonstrated that prestress spatial gradients can lead to the spontaneous nucleation of secondary rupture near the healing tail of a pulse, to back-propagating rupture and to pulse-to-crack transitions, see Figs. 4-5.

The above mentioned rupture phenomena are geophysically documented phenomena of importance, which continue to pose challenges

to our understanding. For example, it is known that while most seismic studies typically only estimate the average rupture velocity, seismic radiation is predominantly affected by the spatiotemporal variation of the rupture velocity (Madariaga, 1977). Our finding, e.g., in relation to the emergence of quasi-periodically propagating slip pulses, can contribute in this context. Moreover, as noted in (Elbanna, 2011), slip pulse propagation and arrest give rise to heterogeneous after-event stresses (cf., top row of Fig. 4) and hence may offer a mechanism for sustaining prestress heterogeneity over many earthquake cycles. Finally, we note that while we mostly considered prestress distributions varying slowly compared to the initial pulse's size, we show in Sect. S-3B in the SM that the lack of scale separation between the prestress spatial variation and the initial size may lead to qualitative changes in the dynamics.

On the more theoretical side, our results demonstrate that the reduced-dimensionality description of unsteady pulses, originally established under uniform prestress conditions (Pomyalov et al., 2023a), is still relevant under some nonuniform prestress conditions. Specifically, it has been shown that such pulse dynamics presented in a plane defined by a pair of pulse properties — e.g., its size $L(t)$ and propagation velocity $c(t)$ —, remain close to a special, previously derived curve $L(c)$. For example, periodically (or quasi-periodically) propagating slip pulses under nonuniform prestress correspond to limit cycles (or quasi-limit cycles) in the $L-c$ plane that remain rather close to the special $L(c)$ curve at all times, see Figs. 2-3 and SM.

Consequently, while the special $L(c)$ curve is not a strict equation of motion for unsteady pulses under nonuniform prestress, in many cases it does provide a good approximation for the dynamics, in the sense that the knowledge of one pulse property, e.g., $c(t)$, can be used to infer another property, e.g., $L(t)$. Finally, we also demonstrated that similarly to the uniform prestress case (Pomyalov et al., 2023a), the emerging theoretical picture remains valid upon using other pairs of pulse properties, e.g., $L(t)$ and the peak slip velocity $v_p(t)$ (see SM). Future work should consider a broader range of prestress distributions, including sharp steps, barriers of various sizes and realistic after-event stress fields.

CRediT authorship contribution statement

Anna Pomyalov: Writing – review & editing, Writing – original draft, Visualization, Investigation, Formal analysis, Conceptualization. **Eran Bouchbinder:** Writing – review & editing, Writing – original draft, Supervision, Project administration, Investigation, Funding acquisition, Formal analysis, Conceptualization.

Code availability

The code used to generate the results presented in this work has been deposited in the Zenodo open research repository at https://zenodo.org/doi/10.5281/zenodo.13997992.

Declaration of competing interest

The authors declare that they have no known competing financial interests or personal relationships that could have appeared to influence the work reported in this paper.

Acknowledgements

We acknowledge support by the Israel Science Foundation (ISF grant no. 1085/20), the Minerva Foundation (with funding from the Federal German Ministry for Education and Research), the Ben May Center for Chemical Theory and Computation, and the Harold Perlman Family. We are grateful to Prof. Eric Dunham for posing to us the basic question, to Dr. Fabian Barras for his help with setting up the initial conditions in cRacklet and to Dr. Efim Brener for useful discussions.

Appendix A. Supplementary material

Supplementary material related to this article can be found online at https://doi.org/10.1016/j.epsl.2024.119111.

Data availability

Data will be made available on request.

References

Aki, K., 1979. Characterization of barriers on an earthquake fault. J. Geophys. Res., Solid Earth 84 (B11), 6140–6148.
Bache, T.C., Lambert, D.G., Barker, T.G., 1980. A source model for the March 28, 1975, Pocatello Valley earthquake from time-domain modeling of teleseismic P waves. Bull. Seismol. Soc. Am. 70 (2), 405–418.
Barras, F., Thøgersen, K., Aharonov, E., Renard, F., 2023. How do earthquakes stop? Insights from a minimal model of frictional rupture. J. Geophys. Res., Solid Earth 128 (8), e2022JB026070.
Baumberger, T., Caroli, C., 2006. Solid friction from stick-slip down to pinning and aging. Adv. Phys. 55, 279–348.
Beroza, G.C., Mikumo, T., 1996. Short slip duration in dynamic rupture in the presence of heterogeneous fault properties. J. Geophys. Res., Solid Earth 101 (B10), 22449–22460.
Brantut, N., Garagash, D.I., Noda, H., 2019. Stability of pulse-like earthquake ruptures. J. Geophys. Res., Solid Earth 124 (8), 8998–9020.
Breitenfeld, M.S., Geubelle, P.H., 1998. Numerical analysis of dynamic debonding under 2D in-plane and 3D loading. Int. J. Fract. 93 (1/4), 13–38.
Brener, E.A., Aldam, M., Barras, F., Molinari, J.F., Bouchbinder, E., 2018. Unstable slip pulses and earthquake nucleation as a nonequilibrium first-order phase transition. Phys. Rev. Lett. 121 (23), 234302.
Das, S., 1980. A numerical method for determination of source time functions for general three-dimensional rupture propagation. Geophys. J. Int. 62 (3), 591–604.
Day, S.M., 1982. Three-dimensional simulation of spontaneous rupture: the effect of nonuniform prestress. Bull. Seismol. Soc. Am. 72 (6A), 1881–1902.
Dieterich, J.H., 1979. Modeling of rock friction: 2. Simulation of preseismic slip. J. Geophys. Res. 84 (B5), 2169.
Ding, X., Xu, S., Fukuyama, E., Yamashita, F., 2024. Back-propagating rupture: nature, excitation, and implications. J. Geophys. Res., Solid Earth 129, e2024JB029629.
Duan, B., Oglesby, D.D., 2007. Nonuniform prestress from prior earthquakes and the effect on dynamics of branched fault systems. J. Geophys. Res., Solid Earth 112, B05308.
Elbanna, A.E., 2011. Pulselike ruptures on strong velocity-weakening frictional interfaces: dynamics and implications. Ph.D. thesis. California Institute of Technology.
Fang, Z., Dunham, E.M., 2013. Additional shear resistance from fault roughness and stress levels on geometrically complex faults. J. Geophys. Res., Solid Earth 118 (7), 3642–3654.
Freund, L.B., 1998. Dynamic Fracture Mechanics. Cambridge University Press, Cambridge.
Gabriel, A.A., Ampuero, J.P., Dalguer, L.A., Mai, P.M., 2012. The transition of dynamic rupture styles in elastic media under velocity-weakening friction. J. Geophys. Res., Solid Earth 117 (B9), B09311.
Hanks, T.C., 1974. The faulting mechanism of the San Fernando earthquake. J. Geophys. Res. 79 (8), 1215–1229.
Hartzell, S., Brune, J.N., 1979. The Horse Canyon earthquake of August 2, 1975—two-stage stress-release process in a strike-slip earthquake. Bull. Seismol. Soc. Am. 69 (4), 1161–1173.
Heaton, T.H., 1990. Evidence for and implications of self-healing pulses of slip in earthquake rupture. Phys. Earth Planet. Inter. 64 (1), 1–20.
Heimisson, E.R., 2020. Crack to pulse transition and magnitude statistics during earthquake cycles on a self-similar rough fault. Earth Planet. Sci. Lett. 537, 116202.
Idini, B., Ampuero, J.P., 2020. Fault-zone damage promotes pulse-like rupture and back-propagating fronts via quasi-static effects. Geophys. Res. Lett. 47 (23), e2020GL090736.
Johnson, E., 1990. On the initiation of unidirectional slip. Geophys. J. Int. 101 (1), 125–132.
Kanamori, H., Stewart, G.S., 1978. Seismological aspects of the Guatemala earthquake of February 4, 1976. J. Geophys. Res., Solid Earth 83 (B7), 3427–3434.
Lozos, J.C., Oglesby, D.D., Duan, B., Wesnousky, S.G., 2011. The effects of double fault bends on rupture propagation: a geometrical parameter study. Bull. Seismol. Soc. Am. 101 (1), 385–398.
Lu, X., Lapusta, N., Rosakis, A.J., 2007. Pulse-like and crack-like ruptures in experiments mimicking crustal earthquakes. Proc. Natl. Acad. Sci. 104 (48), 18931–18936.
Madariaga, R., 1977. High-frequency radiation from crack (stress drop) models of earthquake faulting. Geophys. J. Int. 51 (3), 625–651.
Marone, C., 1998. Laboratory-derived friction laws and their application to seismic faulting. Annu. Rev. Earth Planet. Sci. 26 (1), 643–696.
Matsumoto, S., Yamashita, Y., Nakamoto, M., Miyazaki, M., Sakai, S., Iio, Y., Shimizu, H., Goto, K., Okada, T., Ohzono, M., et al., 2018. Prestate of stress and fault behavior during the 2016 Kumamoto earthquake (M7.3). Geophys. Res. Lett. 45 (2), 637–645.

Mildon, Z., Roberts, G.P., Faure Walker, J., Toda, S., 2019. Coulomb pre-stress and fault bends are ignored yet vital factors for earthquake triggering and hazard. Nat. Commun. 10 (1), 2744.
Nakatani, M., 2001. Conceptual and physical clarification of rate and state friction: frictional sliding as a thermally activated rheology. J. Geophys. Res., Solid Earth 106 (B7), 13347–13380.
Perrin, G., Rice, J.R., Zheng, G., 1995. Self-healing slip pulse on a frictional surface. J. Mech. Phys. Solids 43 (9), 1461–1495.
Pomyalov, A., Barras, F., Roch, T., Brener, E.A., Bouchbinder, E., 2023a. The dynamics of unsteady frictional slip pulses. Proc. Natl. Acad. Sci. 120 (34), e2309374120.
Pomyalov, A., Lubomirsky, Y., Braverman, L., Brener, E.A., Bouchbinder, E., 2023b. Self-healing solitonic slip pulses in frictional systems. Phys. Rev. E 107 (1), L013001.
Rice, J.R., 1980. The mechanics of earthquake rupture. In: Phys. Earth's Inter., pp. 555–649.
Roch, T., Barras, F., Geubelle, P.H., Molinari, J.F., 2022. cRacklet: a spectral boundary integral method library for interfacial rupture simulation. J. Open Sour. Softw. 7 (69), 3724.
Ruina, A.L., 1983. Slip instability and state variable friction laws. J. Geophys. Res. 88 (B12), 10359–10370.
Scholz, C.H., 2002. The Mechanics of Earthquakes and Faulting. Cambridge University Press.